Performance of Swashplateless Ultralight Helicopter Rotor with Trailing-Edge Flaps for Primary Flight Control

Jinwei Shen
Graduate Student
Alfred Gessow Rotorcraft Center
Department of Aerospace Engineering
University of Maryland, College Park, MD

Inderjit Chopra
Alfred Gessow Professor & Director

Wayne Johnson
Aerospace Engineer
Army/NASA Rotorcraft Division
NASA Ames Research Center
Moffett Field, CA

This study evaluates the rotor performance, trailing-edge deflections and actuation requirement of a helicopter rotor with trailing-edge flap for primary flight control. The swashplateless design is implemented by modifying a two-bladed teetering rotor of an ultralight helicopter through the use of plain flaps on the blades, and by replacing the pitch link. A comprehensive rotorcraft analysis based on UMARC is carried out to obtain the results for both the swashplateless and a conventional baseline rotor configuration. The predictions show the swashplateless configuration achieves better performance than the conventional rotor, because of the reduction of parasite drag resulting from eliminating the swashplate mechanical system. The optimal selection of blade pitch index angle, flap location, length, and chord ratio reduces flap deflections and actuation requirements, with virtually no effect on rotor performance.

Notation

C_D	Drag
C_F	Trailing-edge flap force
C_N	Normal force
C_Q	Rotor torque coefficient
C_S	Leading-edge suction force
C_T	Rotor thrust coefficient
C_W	Gross weight coefficient
FM	Figure of merit
M_h	Trailing-edge flap hinge moment
N_b	Number of rotor blades
P_f	Trailing-edge flap actuation power
R	Rotor blade radius
$\frac{dC_l}{d\delta}$	Lift increment sensitivity to flap deflection
$\frac{dC_m}{d\delta}$	Moment increment sensitivity to flap deflection
$\frac{f}{A}$	Parasite drag area ratio
c	Rotor blade chord
r_{mid}	Trailing-edge flap middle section location
α	Angle of attack
δ	Trailing-edge flap deflection
δ_0	Trailing-edge flap collective angle
δ_{1c}	Trailing-edge flap lateral cyclic
δ_{1s}	Trailing-edge flap longitudinal cyclic
$\overset{\star}{\delta}$	Trailing-edge flap rate
η	Leading-edge suction recovery factor
μ	Advance ratio
ψ	Azimuth angle
σ	Rotor solidity
θ	Blade pitch angle
θ_0	Blade collective pitch
θ_{1c}	Blade lateral cyclic pitch
θ_{1s}	Blade longitudinal cyclic pitch
θ_{index}	Blade index angle
θ_{root}	Blade pitch motion at root spring

Introduction

Trailing edge flap systems for primary flight control date back to the earliest days of rotorcraft development (Ref. 1). In the recent years, the emergence of high energy density smart material actuators has led to interest in trailing-edge flaps as means for vibration and noise control (Ref. 2). Several small scale rotors with a trailing-edge flap system actuated by embedded smart materials have been developed by various researchers, including Prechtl and Hall (Ref. 3), Lee and Chopra (Ref. 4), Bernhard and Chopra (Ref. 5), Koratkar and Chopra (Ref. 6), and Fulton and Ormiston (Ref. 7). A full scale rotor with a smart trailing-edge flap system has

been designed by Straub, *et al.* (Ref. 8), and will be tested in flight. Numerical simulations (Refs. 9–11) and wind tunnel experiments (Ref. 6) have shown that helicopter hub vibratory loads can be successfully minimized with active controlled trailing-edge flap systems. It appears a helicopter rotor embedded with a smart trailing-edge flap will enable future rotorcraft to achieve the long desired "jet-smooth" ride and small noise pollution.

The use of a trailing-edge flap rotor for primary flight control appears attractive, again in the context of an actively controlled rotor where embedded flaps can perform multiple functions. A trailing-edge flap system was the primary candidate in the NASA Revolutionary Concepts (RevCon) program of "swashplateless helicopter flight". The conventional helicopter mechanical control system typically consists of rotor swashplate, pitch links and pushrods, and fixed system hydraulic flight control actuators. This system contributes significantly to the weight, drag, and maintenance cost of the aircraft, and hence degrades the overall mission performance, reduces service life, and increases operating cost. Experiments conducted by Barrett *et al.* (Ref. 12) on a model helicopter achieved a 26% reduction in parasitic drag, 40% reduction in flight control system weight, and 8% reduction in total aircraft gross weight by eliminating the swashplate assembly.

There are primarily two types of flaps that are suitable for mounting on helicopter blades: servo flaps and plain flaps. The servo-flap design consists of auxiliary airfoil sections that are located aft of the trailing edge of the main blades. Despite the successful service history of servo-flaps for blade primary control as demonstrated on rotorcraft designed by Kaman (Refs. 13–15), plain flaps are the choices of most of the recently developed actively controlled rotors (Refs. 3, 6–8). This is because plain flaps are easily coupled with the use of smart materials. In this configuration, the flap is integrated into the rotor blade by locating the flap actuation and support structure, hinge, and linkage assembly within the blade profile, resulting in a reduction in aerodynamic drag, and an increase of flap effectiveness by narrowing the hinge gap. The servo flap is somewhat inefficient because of the high drag resulting from exposure of the hinges and supporting structure, and reduction in aerodynamic efficiency caused by the flap hinge gap (Ref. 16). However, compared with servo flaps, plain flaps are located much closer to the blade elastic axis and hence their capability to generate pitching moments is correspondingly reduced.

Lemnios and Wei *et al.* (Refs. 13–15) presented modeling and correlation for Kaman's SH-2 rotor, which utilizes the servo-flap type system as a primary control device. Straub and Charles (Ref. 17) examined the preliminary control requirements of the swashplateless design for an Advanced Rotor and Control System (ARCS) concept. A recent study by Ormiston, using a simple rigid rotor model, explored the feasibility of a swashplateless rotor with plain trailing-edge flaps (Ref. 16). This study concluded that the on-blade trailing-edge flap system has the potential to satisfy general requirements for primary flight control and the profile power penalty associated with flap deflection may be acceptable with the use of pitch indexing (pre-collective). In a recent study, the authors developed a comprehensive analysis (Ref. 18) for a swashplateless rotor with trailing-edge flaps based on UMARC (University of Maryland Advanced Rotorcraft Code) (Ref. 19). The analysis was carried out for a five-bladed bearingless rotor system (MD 900) with a soft pitch link (control frequency of 2.1/rev) for the wind tunnel trim conditions. A swashplateless rotor with plain flaps was shown to be trimmed successfully in the complete range of advance ratios. Furthermore, the required flap angles were found to be moderate with a proper selection of blade pitch index angle. A multicyclic controller was implemented to minimize vibratory hub loads with the swashplateless rotor system. The plain flaps were shown to be capable of performing both primary rotor control and active vibration control functions. Additionally, the authors conducted a numerical parameter study (Ref. 20) for a swashplateless design based on a modern bearingless rotor. Blade pitch index angle, blade root spring stiffness, trailing-edge flap location and size (length and chord ratio) were found to be key parameters in the design of a swashplateless rotor with trailing-edge flaps. Also, the aeroelastic stability characteristics were compared between the swashplateless rotor and conventional swashplate rotor. Overall, the swashplateless rotor was found to be more stable than the conventional rotor. Most recently, the authors (Ref. 21) developed a comprehensive rotorcraft analysis to examine plain trailing-edge flap for primary control of an ultralight helicopter (ASI 496) with two-bladed teetering rotor. The prediction capability of the analysis was correlated with the predictions of another comprehensive analysis (CAMRAD II) (Refs. 22, 23). The correlation was carried out for the baseline rotor without trailing-edge flaps embedded. Good agreement was shown for the predicted blade natural frequencies at different rotor rotating speeds, the rotor pitch angles, main shaft tilt angles and main shaft power. Key design parameters, such as pitch index angle, flap location, flap length and chord ratio, were studied numerically.

The objective of the present study is to evaluate the performance of the teetering rotor of an ultralight helicopter with plain trailing-edge flap system for primary control, and investigate effect of various key design variables such as pitch index angle, flap location and size on rotor performance, trailing-edge flap deflections and

actuation requirement.

Analytical Model

The baseline rotor configuration for the swashplateless configuration is the ASI 496 (Table 1), an ultralight sport helicopter. It utilizes a 2 blade teetering rotor design and has a normal gross weight of 912 lbs and a cruise speed of 61 knots ($\mu = 0.16$). The conventional swashplate controlled system gives a rotating blade torsional frequency of 2.2/rev (Table 2). The present swashplateless rotor design modifies the baseline rotor by replacing the pitch link assembly with a linear root spring, and keeping the torsional frequency the same as the conventional rotor.

The baseline rotor analysis is adapted from UMARC. The modeling of the swashplateless teetering rotor with trailing-edge flaps in free flight steady trim is discussed in Ref. 21. The following briefly outlines the analysis and solution procedure adopted. The analysis incorporates finite element methodology in space and time. In the analysis of the teetering rotor, it is necessary to treat two blades simultaneously because the blades are rigidly connected to each other and attached to the mast through a common flapping hinge (Ref. 24). The blade is modeled as an elastic beam undergoing flap bending, lag bending, elastic twist, and axial deformation. The rotor blades are discretized into a finite number of beam elements, each with 15 degrees of freedom. Nineteen aerodynamic/structural elements are used to model the main blade. The coupled blade response and the trim control settings are solved simultaneously for the propulsive trim condition. Eight time elements with fifth order shape functions are used to calculate the coupled trim solution. The trailing-edge flap motion is prescribed, and as such smart actuator dynamics are neglected for this study (Ref. 25). However, trailing-edge flap aerodynamic and inertial effects are included both in the formulation of the blade equations of motion and the hub loads computation. The Drees linear inflow is used to obtain the induced inflow distribution over the rotor disk.

For a rotor with flaps for primary controls, the control angle input to a flap is given by;

$$\delta(\psi) = \delta_0 + \delta_{1c} \cos \psi + \delta_{1s} \sin \psi \quad (1)$$

and the blade pitch angle consists of the blade index angle plus the pitch induced by flap control inputs;

$$\theta(\psi) = \theta_{index} + \theta_{root}(\psi) \quad (2)$$

The main rotor power is calculated by multiplying hub shaft torque moment with rotor rotating speed, and the hub torque moment is calculated by force summation method.

Table 1: ASI 496 and Trailing-edge Flap Properties

Rotor Type	Teetering
Number of Blades	2
Rotor Diameter	23 ft.
Rotor Speed	525 RPM
Chord	6.7 inch
Linear Twist Angle	-8°
Lock Number	5.01
Solidity	0.0309
C_T/σ	0.075
Undersling	3.45 inch
Weight	912 lb
Cruise Speed	61 knots
CG position	0.75 in forward
Parasite Drag Area Ratio ($\frac{f}{A}$)	0.0315
T.E. Flap Data	
Flap Type	Plain Flap
Spanwise Length	25 inch (0.18R)
Chordwise Size	25 % (Blade Chord)
Flap Midspan Location	0.82R

Figure of merit is calculated in hover by;

$$FM = C_T \sqrt{C_T/2}/C_Q \quad (3)$$

The actuation power of the flap system is calculated by integrating the product of the hinge moment and flap deflection rate over one complete rotor revolution:

$$P_f = \frac{N_b}{2\pi} \int_0^{2\pi} \max(-M_h \overset{\star}{\delta}, 0) d\psi \quad (4)$$

The actuation power presented in equation 4 is "ideal" because it only includes the energy used to drive the flap system, and neglects the heat dissipation of the smart actuators.

The aerodynamic model of an airfoil with a plain trailing-edge flap used in present analysis was developed by Hariharan and Leishman (Ref. 26). This model, based on the Theodorsen model (Ref. 27), uses an indicial method and includes compressibility and unsteady effects. The Hariharan-Leishman model can predict sectional lift, drag, pitching moment, and hinge moment coefficient as a function of flap chord ratio, angle of attack, flap angle, and unsteady airfoil and flap motion. This model resolves the drag into normal forces, flap forces, and leading-edge suction forces:

$$C_D = \alpha C_N + \delta C_F - \eta C_S \quad (5)$$

where an empirical leading edge recovery factor η is applied to account for viscous effects. In 2D steady inviscid incompressible thin-airfoil theory, where η equal to one, the airfoil drag of airfoil with plain trailing-edge

Table 2: Calculated normal mode frequencies for ASI 496 rotor at rotating speed of 525 RPM

Mode	Frequency (per rev)
1st flap	1.11
1st inplane	1.23
1st torsion	2.20
2nd flap	3.09
3rd flap	5.78
2nd inplane	7.42
4th flap	8.72

flap predicted by equation 5 will be zero (D'Alembert's paradox). The leading edge recovery factor used in the analysis is 0.97, and aerodynamic drag coefficient of the baseline airfoil due to skin friction, C_{D0} is added on the prediction by equation 5. Although accurate drag prediction for airfoil with trailing-edge flap is important for rotor performance evaluation, the wind tunnel data are scarce for validation (Ref. 16). The aerodynamic coefficients prediction with three flap deflections, namely neutral, and four degrees upward and downward, at different angles of attack are compared with wind tunnel test data (Ref. 28) in figure 1. Good agreement is seen for lift coefficient, and fair agreement for pitching moment coefficient. Drag predictions qualitatively agree with the test data.

Results and Discussion

The parasite drag area of swashplateless configuration is selected at 0.02678, 15% smaller than that of the conventional benefiting of removing swashplate system. The selected weight for both configurations are 912 lbs which gives a C_W/σ of 0.075 except where noted. The baseline trailing-edge flap characteristics are given in Table 1, and the flap has no aerodynamic balance (Ref. 28) in this study. Trailing-edge flap motion is positive for downward deflection, and hinge moment is positive when its direction is "nose-up" (and "tail-down").

Baseline Swashplateless Rotor

Figure 2 compares conventional and swashplateless rotor control settings for the complete range of advance ratios ($\mu = 0$ to 0.17). The swashplateless rotor has a pitch index angle of 18°, which yields small collective flap at the cruise speed 61 knots ($\mu = 0.16$).

Figure 2(a) presents the trailing-edge flap deflection required to trim the swashplateless rotor. The required flap collective and cyclic angles are shown to be below 4° in the complete range of advance ratios. The trailing-edge flap collective angle, δ_0, is deflected downward for

the complete advance ratio range to bring the blade pitch down. The flap collective angle also generates a cyclically varying pitching moments in forward flight conditions, which produces blade cyclic pitch motion. A downward deflected flap collective and nose-down pitching moments of the baseline airfoil are beneficial for reducing required flap cyclic deflections. The cyclic flap deflections (half peak-to-peak), show small variation for advance ratios below 0.13, and increases rapidly above advance ratio of 0.13.

Figure 2(b) compares the 75%R pitch angles of a conventional and swashplateless rotor. The pitch angle is relative to hub plane, that is, the pitch index angle is included for the swashplateless rotor. As expected, blade pitch angles, both collective and cyclic, are similar for the two configurations. The collective blade pitch of the swashplateless rotor is slightly smaller than the conventional rotor in forward flight conditions. This is because of the smaller parasite drag of the swashplateless configuration and the favorable additional lift that is generated from the downward deflected trailing-edge flaps. The blade longitudinal and lateral cyclic pitch of the swashplateless rotor shows small variation compared with the conventional, because of the parasite drag difference and the additional lift generated by the flap cyclic deflections, δ_{1s} and δ_{1c}.

Figure 2(c) compares main rotor power of the swashplateless and conventional rotors. In high speed forward flight conditions, the swashplateless rotor consumes moderately less power than the conventional, because of the reduced parasite drag of the swashplateless design. In hover and low speed flight conditions, the swashplateless rotor consumes the same or slightly less power.

Figure 2(d) illustrates main rotor shaft tilt angles of both configurations. The swashplateless rotor exhibits smaller forward tilt because of reduction of parasite drag in high speed forward flight. Lateral shaft tilts exhibits slight difference between the two configurations.

Figure 2(e) shows the flap actuation requirements in different flight speeds. The mean values of the hinge moments are generally decided by the flap collective, δ_0. The half peak-to peak values of the hinge moments show small variations at hover and low speed forward flights, and increase largely after advance ratio of 0.13, primarily because of an increment of the trailing-edge flap cyclic, and the aggravation of the unsteady aerodynamic environment.

Figure 2(f) shows the flap actuation power, both the absolute value and as a fraction of main rotor power. This power is essentially zero, because it does not account for the thermodynamic losses of the actuator.

Hover Performance

Figure 3 evaluates the performance of swashplateless and conventional rotors at hover for different weight configurations. The ratio of thrust coefficient to rotor solidity, C_T/σ, are from 0.055 to 0.095 which corresponding to weight from 670 to 1155 lbs.

Figure 3(a) shows the flap collective decreases with higher C_T/σ because of the correspondingly large blade pitch collective requirement as shown in figure 3(b). Flap cyclic was shown with virtually no difference at different C_T/σ. Unlike in forward flight conditions, the flap collective has no effect on blade cyclic pitch, and hence no effect on flap cyclic at hover.

Figure 3(b) compares the blade pitch of swashplateless and conventional rotors, and the difference are very small. As expected, the blade collective pitch angles are increasing with C_T/σ, and the blade cyclic pitch are virtually constant versus C_T/σ.

Figure 3(c) evaluates the performance of swashplateless and conventional rotors with the main shaft power and figure of merit illustrated. The swashplateless rotor consumes slightly less power than the conventional, and has a slightly higher figure of merit in the ranges of C_T/σ. The advantage of swashplateless rotor is possibly because of upload generated by flap collective moves the lift inboard, and results in more uniform blade airloads distribution (Ref. 15).

Figure 3(d) presents the magnitudes of mean hinge moments reduce with C_T/σ because of the decreasing of flap collective angles. Half peak-to-peak hinge moments shows virtually no variation with C_T/σ because the constant flap cyclic and steady aerodynamic environment at hover.

Blade Pitch Index Angle

Figure 4 examines the effect of blade pitch index angle on the flap angle, blade pitch, main rotor power, and flap actuation requirements at an advance ratio of 0.16.

Figure 4(a) shows that the mean values of flap deflection, δ_0, are decreased, because the required blade collective pitch motion is reduced with higher index angle. The flap collective deflection reaches almost zero with a pitch index angle of 17° at an advance ratio of 0.16, and increases thereafter, because the index angle provides more pitch than is needed for steady flight trim (i.e. downward flap deflections would be required). The flap longitudinal cyclic deflection reduces because of the favorable blade cyclic pitch induced by downward flap collective deflection, δ_0, in high forward flight conditions. The effect is smaller on lateral flap cyclic than longitudinal cyclic. The half peak-to-peak of flap deflections decreases with increasing of pitch index angle.

Figure 4(b) illustrates that blade collective pitch decreases slightly with blade index angle because of the additional lift generated by a downward deflected flap collective. Similarly, the lift obtained by cyclic flap inputs alters the blade longitudinal cyclic pitch, and again more on the longitudinal component.

Figure 4(c) presents the main rotor power showing virtually no variation in different blade index angles. This contradicts the expectation because large drag should have been generated with large flap deflections with small blade index angle. In order to give better power prediction, it requires a more accurate aerodynamic drag models.

Figure 4(d) shows the half peak-to-peak value of flap hinge moment changes less because of small variation of cyclic components of blade pitch angle and flap deflections. The mean values vary from a nose-up hinge moment at zero index angle, to a nose-down moment for an index angle below 14°.

Figure 4 suggests an optimal blade pitch index angle of 18° for an advance ratio of 0.16. However, the optimal pitch index angle is varying with advance ratio because of the variation of required blade pitch, and as a result, a compromise is required.

Flap Spanwise Location

Figure 5 examines the effect of flap location on the flap angle and main rotor power at an advance ratio of 0.16. Figure 5(a) shows a reduction in flap collective deflection is achieved by moving the flap spanwise location toward the blade tip. This is because the flap effectiveness increases when the flap is located near the blade tip, where high dynamic pressure exists. Similarly, flap cyclic reduces. Figure. 5(b) presents main rotor power showing no variation with trailing-edge flap locations.

Flap Length

Figure. 6(a) shows both flap collective and cyclic reduce with increasing flap length, because of the increasing of flap effectiveness. Again, main rotor power presents no variation with different trailing-edge flap length (figure 6(b)).

Flap Chord Ratio

Figure 7 examines the effect of flap chord ratio on the flap angle and main rotor power at an advance ratio of 0.16. The flap chord ratio is a key design parameter, because it plays an important role in determining the dominant flap effect; i.e. incremental lift or pitching moment. Previous test data and theoretical predictions related to fixed-wing trailing-edge flaps (Refs. 27, 29) show that the flap pitching moment coefficient reaches a

maximum around a flap chord ratio of 0.26 for a plain trailing-edge flap (Figure 8). As shown in Figure 7(a), both flap collective and cyclic deflection are minimized at 20% airfoil chord. The main rotor power (Figure 7(b)) exhibits no variation with trailing-edge flap chord ratio.

Conclusions

This paper evaluated the performance of an ultralight helicopter rotor with trailing-edge flap as primary flight control, and examined effects of various key design variables such as pitch index angle, flap location and geometry on rotor performance and trailing-edge flap deflections. The following conclusions are subject to the limitations of the analysis and the scope of the study:

1. With the design of baseline trailing-edge flap system, which consists of an $18\%R$ plain flap with 25% chord ratio located at $82\%R$, the trailing-edge flap deflections required to trim the rotor are moderate in the complete range of flight speed. Both flap collective and cyclic deflections are below 4°. Accordingly, actuation requirements are also small.

2. Compared with a conventional swashplate-controlled rotor, the swashplateless configuration consumes moderately less power in high speed forward, because of the 15% reduction in parasite drag assumed for the swashplateless design. In hover and low speed flight conditions, the swashplateless rotor consumes same or slightly less power.

3. Compared with the conventional rotor at various gross weights in hover, the swashplateless rotor consumes slightly less power, and hence shows higher figures of merit.

4. Optimal selection of pitch index angle, flap location, length and chord ratio is key to reduce trailing-edge flap angles and actuation requirement, with virtually no effect on rotor performance.

Acknowledgments

References

[1]Pescara, R. P. "Screw Propeller of Helicopter Flying Machines,". U.S. Patent 1,449,129, March 20, 1923.
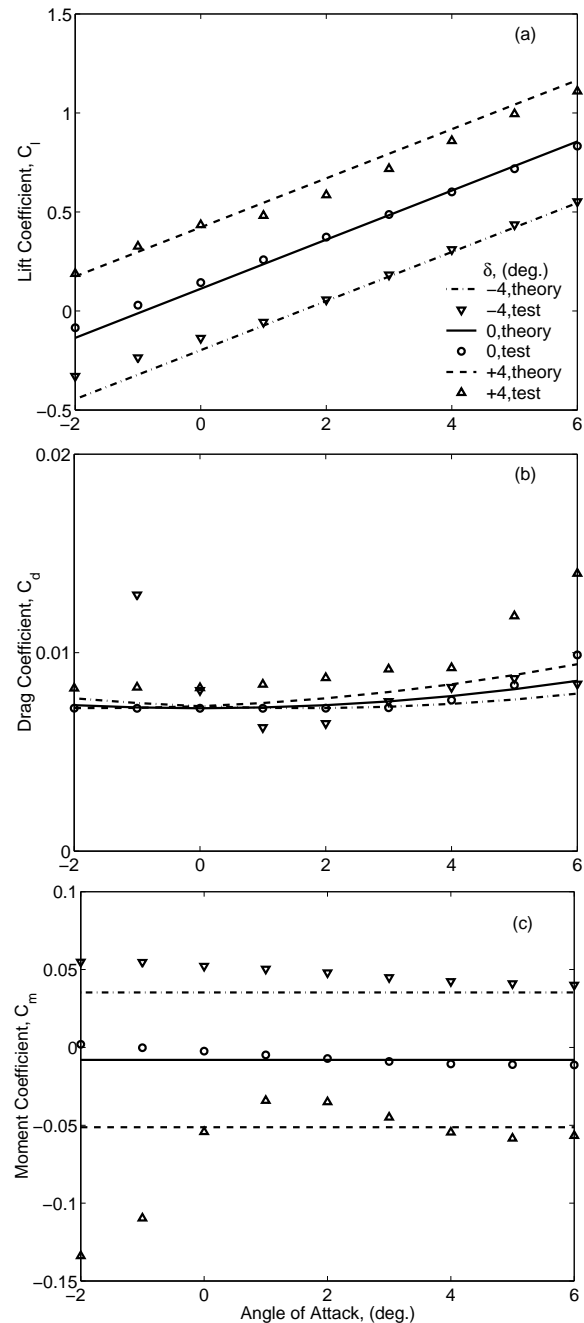

Figure 1: Measured and predicted aerodynamic coefficients of 2D HH-06 airfoil with 0.35 plain trailing-edge flap (10%c overhang, Mach = 0.45); (a) lift (b) drag and (c) pitching moment
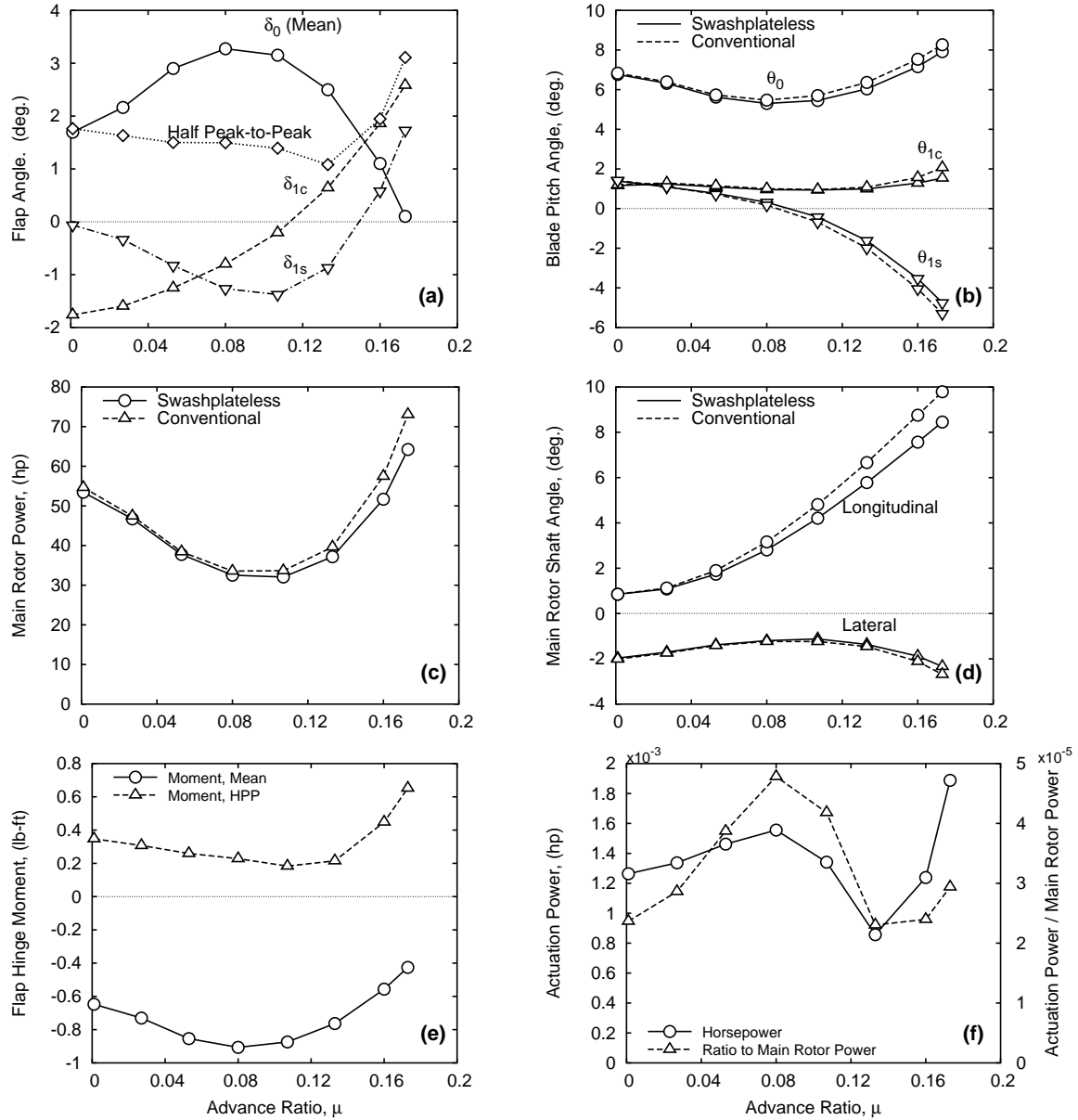
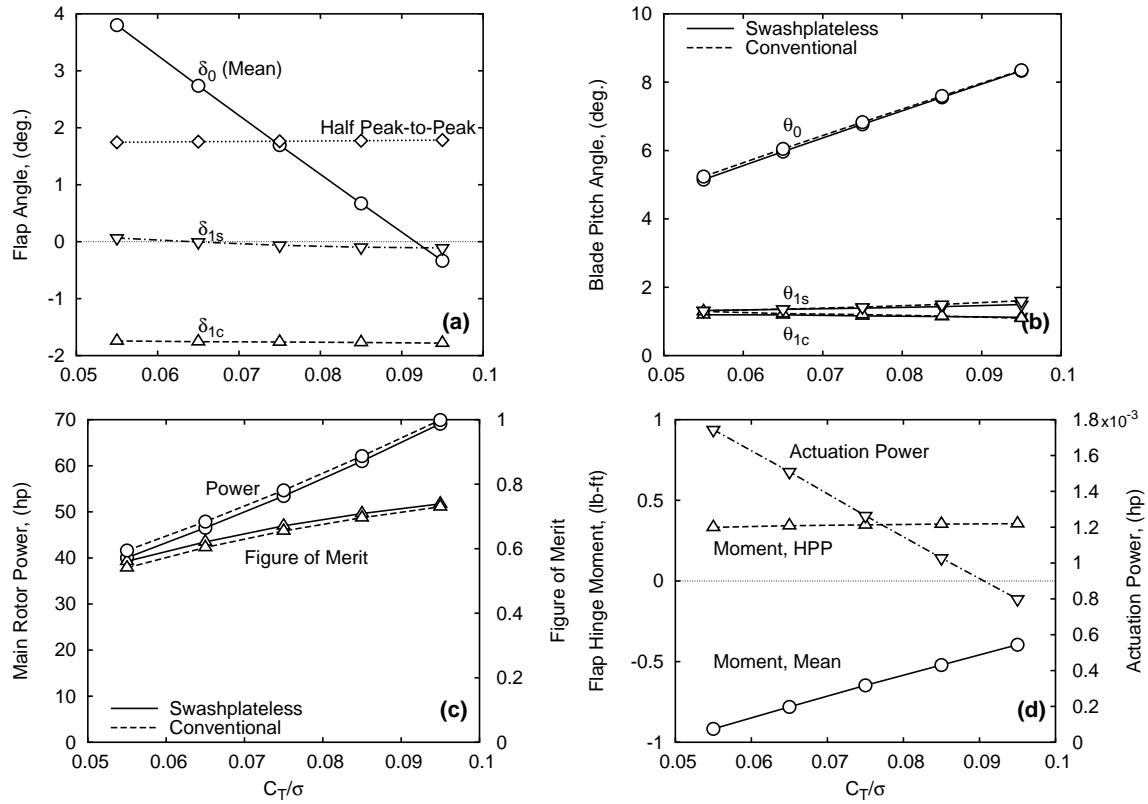Figure 2: Comparisons of conventional and swashplateless rotor at different forward speeds

Figure 3: Comparisons of conventional and swashplateless rotors for different thrust levels at hover
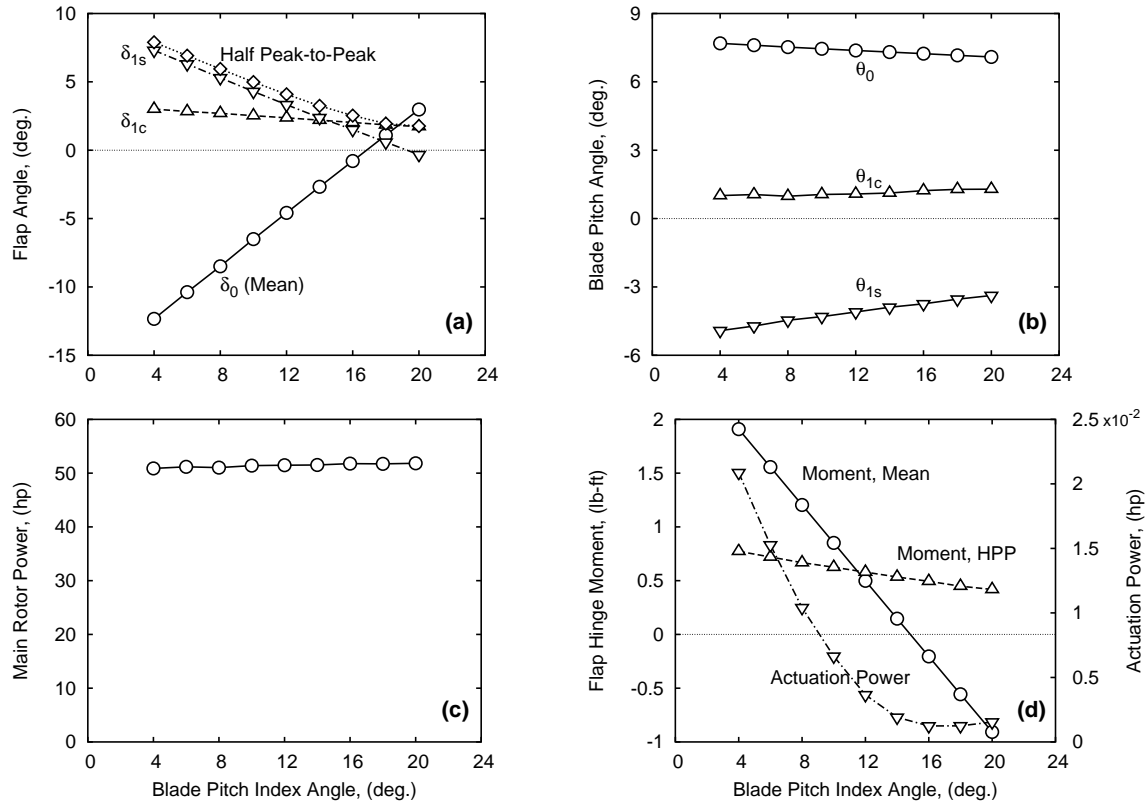

Figure 4: Effect of pitch index angle on trailing-edge flap angles, main rotor power, and and actuation requirements at forward speed of 60 knots ($\mu = 0.16$)
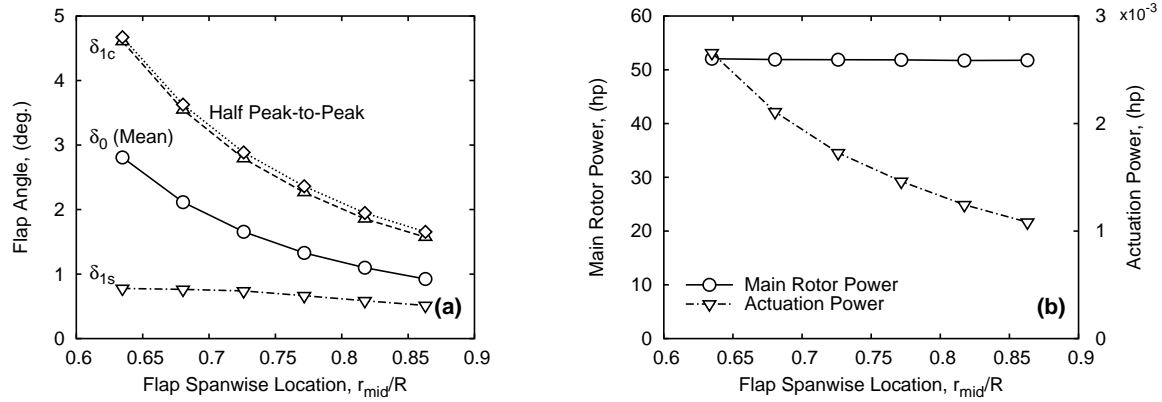
Figure 5: Effect of trailing-edge flap location on flap angles, main rotor power, and and actuation requirements at forward speed of 60 knots ($\mu = 0.16$)
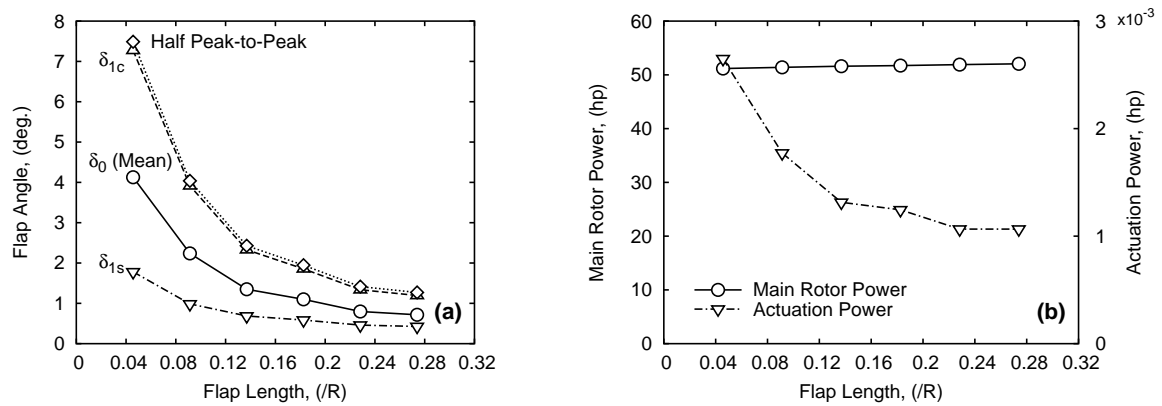

Figure 6: Effect of trailing-edge flap length on flap angles, main rotor power, and and actuation requirements at forward speed of 60 knots ($\mu = 0.16$)
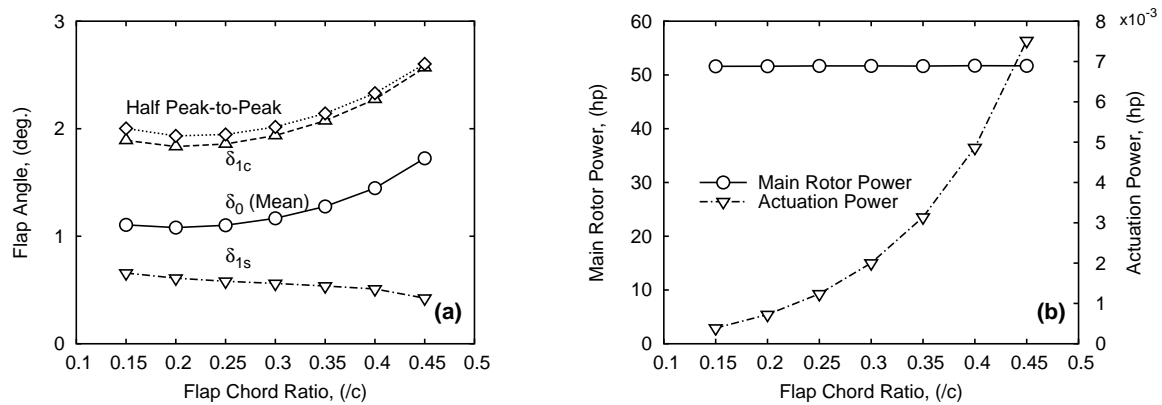

Figure 7: Effect of trailing-edge flap chord ratio on flap angles, main rotor power, and and actuation requirements at forward speed of 60 knots ($\mu = 0.16$)

[2]Chopra, I., "Status of Application of Smart Structures Technology to Rotorcraft Systems," *Journal of the American Helicopter Society*, Vol. 45, (4):228–252, October 2000.

[3]Prechtl, E. and Hall, S. "An X-frame Actuator Servo-Flap Actuation System for Rotor Control,". In *SPIE Symposium on Smart Structures and Materials, Conference on Smart Structures and Integrated Systems*, San Diego, CA, March 1998.

[4]Lee, T. and Chopra, I. "Design of a Bidirectional Piezoelectric Actuator for Blade Trailing-Edge Flap,". In *SPIE Symposium on Smart Structures and Materials, Conference on Smart Structures and Integrated Systems*, number 4327-05, Newport Beach, CA, March 2001.

[5]Bernhard, A. and Chopra, I., "Trailing Edge Flap Activated by a Piezo-Induced Bending-Torsion Coupled Beam," *Journal of the American Helicopter Society*, Vol. 44, (1):3–15, January 1999.

[6]Koratkar, N. A. and Chopra, I., "Wind Tunnel Testing of a Mach-Scaled Rotor Model with Trailing-Edge Flaps," *Journal of the American Helicopter Society*, Vol. 47, (4):263–272, October 2002.

[7]Fulton, M. V. and Ormiston, R. A., "Hover Testing of a Small-Scale Rotor with On-Blade Elevons," *Journal of the American Helicopter Society*, Vol. 46, (2):96–106, Apri 2001.

[8]Straub, F. K. and Charles, B. D., "Aeroelastic Analysis of Rotors with Trailing Edge Flaps Using Comprehensive Codes," *Journal of the American Helicopter Society*, Vol. 46, (3):192–199, July 2001.

[9]Millott, T. and Friedmann, P. "Vibration Reduction in Helicopter Rotors Using an Actively Controlled Partial Span Trailing Edge Flap Located on the Blades," Technical Report CR 4611, NASA, June 1994.

[10]Milgram, J., Chopra, I., and Straub, F., "Rotors with Trailing Edge Flaps: Analysis and Comparison with Experiment Data," *Journal of the American Helicopter Society*, Vol. 43, (4):319–332, October 1998.

[11]Shen, J. and Chopra, I. "Aeroelastic Modeling of Trailing-Edge Flaps with Smart Material Actuators,". In *Proceedings of the 41st AIAA/ASME/ASCE/AHS/ASC structure, structural dynamics, and materials conference*, AIAA-2000-1622, page 14, Atlanta, GA, April, 3-6 2000.

[12]Barrett, R., Schliesman, M., and Frye, P. "Design, Development and Testing of a Mini Solid State Adaptive Rotorcraft,". In *SPIE Symposium on Smart Structures and Materials, Conference on Smart Structures and Integrated Systems*, pages 231–242, San Diego, CA, March 1997.
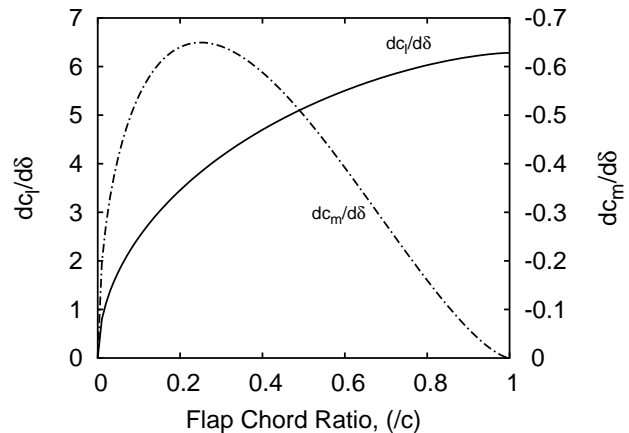
Figure 8: Theoretical lift and pitching moment characteristics of plain trailing-edge flaps

[13]Lemnios, A. Z. and Jones, R. "The Servo Flap – An Advanced Rotor Control System,". In *Proceedings of AHS and NASA Ames Research Center Vertical Lift Aircraft Design Conference*, San Francisco, CA, January, 17-19 1990.

[14]Wei, F.-S. and Jones, R., "Correlation and Analysis for SH-2F 101 Rotor," *Journal of Aircraft*, Vol. 25, (7):647–652, July 1988.

[15]Wei, F.-S. J. and Gallagher, F. "Servo-Flap Rotor Performance Flight Testing and Data Identification,". In *Proceedings of the 57th Annual Forum of the American Helicopter Society*, pages 596–603, Washington, DC, May 2001.

[16]Ormiston, R. A. "Aeroelastic Considerations for Rotorcraft Primary Control with On-Blade Elevons,". In *Proceedings of the 57th Annual Forum of the American Helicopter Society*, Washington, DC, May 2001.

[17]Straub, F. and Charles, B. "Preliminary Assessment of Advanced Rotor/Control System Concepts (ARCS)," Technical Report 90-D03, USA AVSCOM, 1990.

[18]Shen, J. and Chopra, I. "Actuation Requirements for a Swashplateless Helicopter Control System With Trailing-Edge Flaps,". In *Proceeding of the 43rd AIAA/ASME/ASCE/AHS structures, structural dynamics, and materials conference and 10th AIAA/ASME/AHS adaptive structures conference*, number AIAA-2002-1444, page 11, Denver, Colorado, April 2002.

[19]Bir, G., Chopra, I., and et al. "University of Maryland Advanced Rotor Code (UMARC) Theory Manual," Technical Report UM-AERO 94-18, Center for Rotorcraft Education and Research, University of Maryland, College Park, July 1994.

[20] Shen, J. and Chopra, I. "A Parametric Design Study for a Swashplateless Helicopter Rotor with Trailing-Edge Flaps,". In *Proceedings of the AHS* 58th *Annual Forum*, page 15, Montreal, Canada, June 2002.

[21] Shen, J. and Chopra, I. "Ultralight Helicopter with Trailing-Edge Flap for Primary Control,". In *Proceedings of American Helicopter Society International Meeting on Advanced Rotorcraft Technology and Life Saving Activities*, page 10, Tochigi, Japan, November 2002.

[22] Johnson, W. "Rotorcraft Dynamics Models for a Comprehensive Analysis,". In *Proceedings of the* 54th *Annual Forum of the American Helicopter Society*, Washington, DC, May 1998.

[23] Johnson, W. "Rotorcraft Aerodynamics Models for a Comprehensive Analysis,". In *Proceedings of the* 54th *Annual Forum of the American Helicopter Society*, Washington, DC, May 1998.

[24] Yeo, H. *A comprehensive vibration analysis of a coupled rotor/fuselage system*. PhD thesis, University of Maryland, College Park, MD, 1999.

[25] Shen, J. and Chopra, I. "Aeroelastic Stability of Smart Trailing-Edge Flap Helicopter Rotors,". In *Proceedings of the* 42nd *AIAA/ASME/ASCE/AHS/ASC structure, structural dynamics, and materials conference*, AIAA-2001-1675, page 11, Seattle, WA, April, 16-19 2001.

[26] Hariharan, N. and Leishman, J. G. "Unsteady Aerodynamics of a Flapped Airfoil in Subsonic Flow by Indicial Concepts,". In *Proceedings of the the* 36th *AIAA/ASME/ASCE/AHS/ASC structure, structural dynamics, and materials conference*, New Orleans, LA, April 1995.

[27] Theodorsen, T. and Garrick, I. E. "Nonstationary Flow about a Wing-Aileron-Tab Combination Including Aerodynamic Balance," Technical Report No. 736, NACA, 1942.

[28] Hassan, A. A., Straub, F. K., and Noonan, K. W. "Experimental/Numerical Evaluation of Integral Trailing Edge Flaps for Helicopter Rotor Applications,". In *Proceedings of the American Helicopter Society 56th Annual Forum*, page 19, Virginia beach, VA, May, 2-4 2000.

[29] Hoerner, S. F. and Borst, H. V. *Fluid-Dynamic Lift*, chapter Characteristics of airplane control surfaces. Hoerner fluid dynamics, 1975.